The Cryosphere Discuss., https://doi.org/10.5194/tc-2019-46
Manuscript under review for journal The Cryosphere
Discussion started: 3 April 2019

The Cryosphere Discussions
Open Access
EGU

Calving cycle of the Brunt Ice Shelf, Antarctica, driven by changes in ice-shelf geometry

Jan De Rydt[1], G. Hilmar Gudmundsson[1], Thomas Nagler[2], Jan Wuite[2]

[1]Department of Geography and Environmental Sciences, Northumbria University, Newcastle upon Tyne, UK.
[2]ENVEO – Environmental Earth Observation, Innsbruck, Austria.

Correspondence to: Jan De Rydt (jan.rydt@northumbria.ac.uk)

Abstract. Despite the potentially detrimental impact of large-scale calving events on the geometry and ice flow of the Antarctic Ice Sheet, little is known about the processes that drive rift formation prior to calving, or what controls the timing of these events. The Brunt Ice Shelf in East Antarctica presents a rare natural laboratory to study these processes, following the recent formation of two rifts, each now exceeding 50 km in length. Here we use a unique 50-years' time series of in-situ and remote sensing observations, together with numerical modelling, to reveal how slow changes in ice shelf geometry over time caused build-up of mechanical tension far upstream of the ice front, and culminated in rift formation and a significant speed-up of the ice shelf. These internal feedbacks, whereby ice shelves generate the very conditions that lead to their own (partial) disintegration are currently missing from ice flow models, which severely limits their ability to accurately predict future sea level rise.

1 Introduction

Icebergs that calve from the floating margins of the Antarctic Ice Sheet account for up to 50% of ice discharge into the Southern Ocean (Depoorter et al., 2013). The largest calving events, such as the loss of a 5000 km^2 iceberg from the Larsen C Ice Shelf in 2017 (Hogg and Gudmundsson, 2017), result from the horizontal lengthening of multi-kilometre long rifts that cut through the full thickness of the ice. These large-scale events, in contrast to the loss of small ice blocks in the bending zone near the ice front (Reeh, 1968), significantly reshape the geometry of the ice-shelf margins, and can have a profound impact on their structural integrity (Doake et al., 1998). Since ice shelves act as a barrier around the grounded ice and buttress its seaward flow through lateral drag and local grounding in shallow water (Dupont and Alley, 2005), any loss of buttressing around the periphery of Antarctica as a result of calving-induced changes in ice-shelf geometry will adversely affect glacier flow (Scambos et al., 2004, Rignot et al., 2004, Rott et al., 2011), and induce additional ice discharge into the Southern Ocean.

Despite their importance for the mass balance of the Antarctic Ice Sheet, detailed observations of calving events and related changes in ice-shelf dynamics remain scarce. In particular, conditions for full-depth fracture and the subsequent propagation of kilometre-scale rifts are poorly understood. Based on limited observations, rifts have been shown to lengthen at rates that

vary strongly in time (Bassis et al., 2005, Borstad et al., 2017, De Rydt et al., 2018), from meters to kilometres per day, and can arrest for extended periods. Suture zones of basally accreted marine ice have been linked to periods of slow rift propagation and could delay or halt large-scale calving (Borstad et al., 2017). Contrasting observations have reported fast unzipping of rifts along bands of marine ice and slow propagation through meteoric ice (De Rydt et al., 2018, King et al., 2018), highlighting the complex nature of rift behaviour. At present, a unified formulation of rift dynamics rooted in existing theory of fracture mechanics is still under development (Rist et al., 2002, Bassis et al., 2008, Lipovsky, 2018a,b). As a result, predictions for the location and timing of large-scale calving events remain ill-constrained and the feedback between calving rates and ongoing climate-change induced thinning of ice shelves (Pritchard et al., 2009, Flament and Remy, 2012, Konrad et al., 2016) is unknown.

Fortuitously, a unique opportunity to enhance our process-based understanding of rift dynamics and calving has recently arisen with the impending calving of two tabular icebergs from the Brunt Ice Shelf (BIS) in East Antarctica (Figure 1a). In December 2012 a historical rift structure, 'Chasm 1', that had lain dormant for three decades (Figure 1b), was reactivated and started to lengthen by several kilometres per year (De Rydt et al., 2018). Chasm 1 still continues to grow to date. The renewed rifting activity was followed by the formation of a second rift, the so-called 'Halloween Crack' in October 2016 (De Rydt et al., 2018), which grew quickly and reached a length of 60 km by October 2018 (Figure 1b).

The behaviour of both rifts has been documented in great detail since the day of their initiation, in part by an extensive, and for Antarctic ice shelves, unique, network of up to 15 GPS stations on the BIS (Gudmundsson et al., 2017, De Rydt et al., 2018). Furthermore, recent advances in satellite data availability have provided a comprehensive spatial and temporal description of the flow and ice deformation across the ice shelf (Thomas, 1973, Simmons and Rouse, 1984, Simmons, 1986, Gudmundsson et al., 2017). In addition, the continuous occupation of the Halley Research Station on the ice shelf since the mid-1950s has allowed us to put ongoing changes into a historical perspective. Here we use these observations, in combination with ice-flow modelling, to understand the conditions that gave rise to the ongoing rifting activity on the ice shelf, and to establish the mechanical properties governing subsequent rift propagation.

2 Ice shelf calving cycle

In the early 1970s, a singular calving event significantly reduced the extent of the BIS (Thomas, 1973), and the retreat of the ice front caused a loss of contact between the ice base and a seabed shoal at the McDonald Ice Rumples (MIR, Figure 1a). The resulting reduction in buttressing (or backstress) coincided with a twofold increase in flow speed of the remainder of the ice shelf (Simmons and Rouse, 1984, Gudmundsson et al., 2017), unequivocally demonstrating the potential impact of geometrical changes on ice-shelf dynamics. In decades following, the ice front re-advanced by up to 30 km in places (Figure 1b) and the

deforming ice gradually re-established ice-to-bed contact at the MIR, causing the ice shelf to slow down to pre-calving speeds by 2012 (Gudmundsson et al., 2017).

The dramatic succession of speed-up and slow-down by over 100% within a few decades comprises some of the highest amplitude variations in flow speed observed in Antarctica, and we argue that these changes are driven entirely by internal ice dynamics processes. The BIS, which is situated on the eastern edge of the Weddell Sea, has not been affected noticeably by changes in external conditions during recent decades. Sustained negative surface temperatures throughout the year prevent surface melting (Anderson et al., 2014) and eliminate the risk of crevasse penetration caused by hydrofracturing (Scambos et al., 2000). There is no indication that offshore Modified Warm Deep Water intrudes into the ice shelf cavity to cause significant basal ablation (Nicholls et al., 2009) or ice-shelf thinning (Paolo et al, 2015). As a result, the BIS represents a unique setting in which large-scale calving processes can be studied in relative isolation, and the wealth of available data can be probed to gain unbiased insights into the universal mechanics of ice-shelf fractures.

In 2012, following four decades of ice shelf growth, the icefront of the BIS reached its most advanced position since the beginning of measurements in 1915 (Anderson et al., 2014). At the same time, preconditions for rifting were re-established, and the reactivation of Chasm 1 in December 2012 and formation of the Halloween Crack in October 2016 marked the start of two new calving events. Their combined impact is expected to reduce the ice shelf's area by more than 50% (De Rydt et al., 2018), the largest singular perturbation in ice shelf geometry on record. In response to the damage caused, a renewed increase in flow speed by up to 10% per year was observed between 2012 and present-day across most of the ice shelf (Figure 1b, (Gudmundsson et al., 2017)).

We note that recent observations of widespread thinning and speed-up of ice shelves in West Antarctica (Pritchard et al, 2012, Flament et al., 2012, Wouters et al., 2015, Konrad et al., 2016) and the complete collapse of some ice shelves along the Antarctic Peninsula (Scambos et al., 2004, Rott et al., 2011), are likely driven by changes in external forcing, such as atmospheric warming or variations in the heat content of the ambient ocean. Whereas these processes warrant timely investigation, and are likely to influence the calving cycle of ice shelves, our focus is on the more commonly neglected internal drivers that underlie rift initiation and propagation. In order to diagnose the timing and location of rifting in relation to internal changes in ice shelf dynamics, we examined stress patterns for 9 different configurations of the BIS between 1997 and 2018 (Table 1).

The Cryosphere Discuss., https://doi.org/10.5194/tc-2019-46
Manuscript under review for journal The Cryosphere
Discussion started: 3 April 2019

3 Data and methods

3.1 Calculation of horizontal stresses

We inferred horizontal components of the stress tensor from the assimilation of the ice shelf geometry and remotely sensed and ground truthed surface velocity and ice thickness data into the SSA (shallow shelf approximation) model Úa (Gudmundsson et al, 2012). The material rheology was described by Glen's Law, $\dot{\epsilon} = A\tau_E^{n-1}\tau$, relating strain rates $\dot{\epsilon}$ to deviatoric stress τ via a power law with creep exponent n=3 and spatially variable rate factor $A(x,y)$. For each geometry, an iterative optimization (or inversion) method with Tikhonov regularization was used to estimate optimal values for the rate factor A by minimizing the mismatch between observed and modelled ice velocities. Based on the diagnostic model output, each ice-shelf configuration was analysed for its instantaneous stress pattern.

The computational domain included the Brunt Ice Shelf and Stancomb Wills Glacier Tongue, similar to (Gudmundsson et al, 2017, De Rydt et al., 2018), in order to fully account for the weak mechanical coupling between both. Only results for the Brunt Ice Shelf are presented here. The unstructured computational mesh for each ice shelf geometry was generated using MESH2D (Engwirda, 2014), and consisted of linear elements with 6 integration points and a mean nodal spacing of 325 m with local mesh refinement down to 100 m nodal spacing around the McDonald Ice Rumples. Dirichlet boundary conditions were imposed for velocities at the grounding line. Optimal values for the Tikhonov regularization multipliers in the inversion ($\boldsymbol{\gamma_s}$ and $\boldsymbol{\gamma_a}$ in (Reese et al., 2018)) were determined using an L-curve approach, and $\hat{\boldsymbol{\gamma}}_{\boldsymbol{a}}$= 1, $\hat{\boldsymbol{\gamma}}_{\boldsymbol{s}}$= 10000 m were found to produce the smallest misfit between observed and modelled surface velocities, whilst limiting the risk of overfitting. The optimal values, $\hat{\boldsymbol{\gamma}}_{\boldsymbol{a}}$ and $\hat{\boldsymbol{\gamma}}_{\boldsymbol{s}}$, were found to be independent of the creep exponent n. Model inversions for different values of the creep exponent (n=2 and n=4) were carried out and results for the stress patterns (not shown) were found to be robust within the observational range of values for n (Cuffey and Paterson, 2010). Inversions for $\mathbf{10} \times \hat{\boldsymbol{\gamma}}_{\boldsymbol{s}}$ and $\hat{\boldsymbol{\gamma}}_{\boldsymbol{s}}/\mathbf{10}$ (not shown) did not lead to any significant changes in the diagnostic stress patterns, and changes to the magnitude of the stress components were limited to less than 10%.

3.2 Observational datasets

In total, 9 different ice shelf configurations between 1997 and 2018 were analysed. Details about the three key observational datasets (ice thickness, surface velocity and ice-shelf geometry) used in the inversion are presented in Table 1. Additional data, in particular MEaSUREs and Sentinel-1 velocity fields, are available and can be used to obtain a denser time series of stress patterns. However, analysis of the additional data does not contain any new findings beyond those presented.

Ice thickness estimates were derived from a digital elevation model (DEM) and a flotation criterion assuming a two-layer density model with a 30-m firn layer (ρ_{firn}= 750 kg/m^3) overlaying solid ice (ρ_{ice}= 920 kg/m^3) (De Rydt et al., 2018). For the 01/01/1999 stress calculation, the Bedmap 2 surface DEM was used. For all other stress calculations, a new DEM was generated from a mosaic of 3m horizontal resolution WorldView-2 tiles acquired between 19 October 2012 and 30 March 2014 (covering the Brunt Ice Shelf) and Cryosat-2 data (Slater et al., 2018) (covering the Stancomb-Wills Glacier Tongue). All WorldView-2 tiles were shifted to a common datum using a surface velocity field from June 2015, and a constant vertical shift was applied to minimize the misfit in overlapping regions. The resulting surface DEM was compared to 5000 km of in situ airborne LiDAR data acquired in January 2017 (Hodgson et al., 2019) and referenced with respect to sea level using 8 LiDAR sections over the open ocean. The mean difference between the resulting DEM and LiDAR data in overlapping regions was 0.01±3.6 m. Prior to each stress calculation, the DEM was shifted to an effective timestamp (first column in Table 1), which corresponds to the middle of the feature tracking window used for the calculation of the surface velocity.

Surface velocity data were acquired from a variety of sources, as detailed in Table 1. Velocity fields based on Sentinel-1 data were processed using an iterative offset tracking method (Nagler et al., 2015). To account for tidal artefacts, all velocity maps were cross-calibrated to high-precision GPS data from a long-term network of up to 15 dual frequency GPS receivers on the Brunt Ice Shelf (Anderson et al., 2014, Gudmundsson et al., 2017, De Rydt et al., 2018). The GPS data were processed using PPP techniques using the Bernese software to obtain daily positions with sub-centimetre precision. For each horizontal velocity component, a linear regression between satellite data and GPS displacements over the corresponding satellite acquisition period was used to calculate the mean offset between both datasets. The offset was subtracted from satellite-derived estimates of surface velocity in order to ensure an optimal fit between the latter and in situ GPS data.

Ice front geometries were outlined from Landsat-7/8 cloud-free panchromatic band images (Table 1). The extent of grounding at the McDonald Ice Rumples was derived from a combination of proxy indicators, in particular crevasse patterns, surface velocity data and surface elevation.

4 Geometrical deformation causes ice-shelf rifting

Figure 2 shows a time series of principal stress directions (arrows) and maximal principal deviatoric stress (colours) in the horizontal plane, covering 12 years before to 4 years after the reactivation of Chasm 1 in December 2012. Before 2000 (Figure 2a), the stress pattern is characteristic for a nearly free floating (or unbuttressed) ice shelf, with most areas showing extensive deviatoric stresses in both principal directions. Between 2000 and 2007 (Figure 2b), a fast and sharp transition occurred from a purely tensile to a mixed tensile/compressive regime, with compressive stress trajectories radially aligned around the MIR. This pattern is characteristic of a point pressure source located at the MIR, and supports the notion that growing contact between the ice base and sea floor caused an increase in backpressure in this area. With the onset of compression, tensile

stresses increased by more than twofold, with the largest values found 10 km upstream of the MIR. Between 2007 and 2013 (Figure 2c), the zone of high tension expanded and spread outward from the MIR, with values up to 110 kPa. Once the periphery of this zone reached the historical rift tip of Chasm 1 in December 2012, the ice shelf eventually fractured along this line of pre-existing weakness (Figure 2c).

After the initiation and sub-critical propagation of Chasm 1 in December 2012, stress values on the western shelf significantly reduced between 2013 and 2016. Simultaneously, bands of high tension developed towards the east of the MIR (Figure 2d) with estimated tensile deviatoric stress values up to 160 kPa. These bands show no obvious spatial correlation to variations in ice thickness or internal ice structure (King et al., 2018). On 4 October 2016, the ice shelf fractured within the band nearest and about 15 km upstream of the MIR (Figure 2d). Following rift initiation, the Halloween Crack rapidly propagated towards the MIR and in the opposing eastward direction along trajectories perpendicular to the local maximal tensile stress direction (Figure 3b and e).

Our numerical simulations provide a simple and intuitive explanation for the sudden reactivation of Chasm 1 in December 2012 and the formation of the Halloween Crack in October 2016. The timing of both rift initiations, the location and the subsequent propagation paths can all be explained in relation to the magnitude and orientation of the tensile deviatoric stress distribution (Figure 2). In both cases, the rifts formed in response to a gradual build-up of horizontal stresses that took place over decades as the ice shelf grew over time. The locations of initiation were consistent with the hypothesis that ice-shelf areas subjected to the highest tensile stress are most susceptible to failure. A priori, these favourable conditions, dictated by changes in geometry, are not restricted to areas close to the ice front or within the shear margins. In particular, they can occur landward of the compressive arch, which is the transition zone between freely floating (or passive) ice close to the ice front, and upstream ice in compression (Doake et al., 1998, Fürst et al., 2016). Rifts that cut through the compressive arch, as is the case for the Halloween Crack, will affect the buttressing capacity of the ice shelf, and thereby induce changes in ice shelf dynamics or continue to affect its structural integrity (Doake et al., 1998).

5 Discontinuous rift propagation

Together with sustained geometrical deformation and ocean pressure acting on newly formed rift surfaces, the reduction in load-bearing capacity of the ice shelf due to rift formation caused a progressive concentration and intensification of the background stress field ahead of the fracture tips. As previously noted, the formation of Chasm 1 caused an increase in horizontal stress towards the south and east of the MIR, which likely contributed to the formation of the Halloween Crack (Figures 2c-d).

Following the initiation of both rifts, further episodes of stress intensification were observed. In early December 2016, following a 4-week period of persistent rift widening but limited changes in rift length (De Rydt et al., 2018), the tip of the Halloween Crack approached a prominent zone of high tensile stress (Figure 3a). The high concentration of remotely-applied stress induced a period of fast propagation, which started around 15 December 2016. By 29 December 2016, the Halloween Crack had propagated a further 11 kilometres at an average rate of 800m/day (compared to <100m/day in November). Following this event, a significant reduction in the calculated tensile stress (Figure 3b) indicated an efficient release of stress through fracture propagation.

A similar event was observed between January 2017 and October 2017 at the tip of Chasm 1. Preceding this period, the location of the fracture tip remained relatively stationary for about 12 months, whereas GPS stations located on both sides of the rift indicated a slowly accelerating increase in its aperture (De Rydt et al., 2018). This allowed a build-up of tensile deviatoric stress ahead of the tip (Figure 3c and d) with values estimated up to 140 kPa. In 2017, a phase of rapid propagation followed, the onset of which was detected in January 2017 (De Rydt et al., 2018). By late October 2017, Chasm 1 had lengthened by about 4.5 km (Figure 3e), and a significant dissipation of stress was again observed. However, given the difficulty in obtaining reliable length measurements of the rift during austral winter and the sparsity of high-quality velocity fields during this time period, the exact timing and rate of propagation remains unknown.

In both occasions, we interpret the results as discontinuous (or episodic) rift propagation controlled by the heterogeneous structure of the ice shelf. The relatively stagnant phases occurred when the fracture tips encountered zones of thick meteoric ice with different mechanical properties (King et al., 2018), causing a temporary fracture arrest and allowing the build-up of the background tensile stress. Once the tension exceeded conditions for rift propagation, a phase of rapid lengthening and stress release followed. Results suggest that discontinuous rift propagation can be expected for all Antarctic ice shelves with heterogeneous properties, and unknown spatial variations in mechanical properties of the ice can lead to significant uncertainties in the timing of fracture initiation and the speed of rift propagation.

Our model results show that by October 2018, the accumulated damage to the BIS had resulted in a significant loss of mechanical coupling between the grounded ice at the MIR and the upstream ice shelf. This loss of mechanical contact provides an explanation for the overall reduction in compressive and tensile stress across the ice shelf (Figure 3b and e). In the near future, the details of the newly emerging ice shelf configuration will depend on the exact pathways of rift propagation (De Rydt et al., 2018, Hodgson et al., 2019). In the most likely scenario, the ice shelf will approach its pre-2000 configuration with a (close-to) freely floating ice tongue, hence completing a 50-year calving cycle that started after the last calving event in the 1970s. However, the potentially complex interaction between two active rifts, and the nascent loss of the largest area of ice since records began in 1915, result in an uncertain future for the ice shelf.

The Cryosphere Discuss., https://doi.org/10.5194/tc-2019-46
Manuscript under review for journal The Cryosphere
Discussion started: 3 April 2019

6 Model simulations of ice dynamics changes

The two characteristic phases in the life-cycle of the BIS (stress accumulation and release) are highly representative for many present-day buttressed ice shelves in Antarctica, and it is imperative that numerical ice-flow simulations are able to represent both phases with confidence in order to make robust projections of Antarctica's future ice-shelf extent and flow.

In order to verify the capability of state-of-the-art ice flow models to reproduce changes in flow speed during a phase of stress accumulation, i.e. before rifting, we used the ice flow model Úa in a time-evolving (transient) mode. Transient model simulations were started from the 2000 ice shelf configuration, with estimates of the rate factor $A(x,y)$ obtained from the corresponding inversion to ensure an optimal fit between the observed and simulated surface velocities, as shown in Figure 4a. The initial rate factor was kept fixed in space throughout all transient simulations, and any changes in ice flow that could result from the advection of A with the ice were therefore ignored. The computational domain was artificially extruded into the open ocean towards the north of the BIS, and covered with a thin layer of ice with a uniform thickness of 1 m and a constant rate factor $A = 3.5\times10^{-25}\text{s}^{-1}\text{Pa}^{-3}$, corresponding to ice at -10°C (Cuffey and Paterson, 2010). The thin ice cover had limited effect on the initial dynamics of the ice shelf, and the enlarged computational domain allowed the ice front to advance beyond its original location.

After 10 years of transient evolution, during which the ice shelf geometry, ice thickness and flow velocities were allowed to freely evolve, the magnitude and spatial distribution of simulated changes in surface speed remained largely consistent with observations (Figure 4b). In particular, growth of the ice shelf caused enhanced ice-bed contact at the MIR both in the observational data set and the numerical simulations. The increasing amount of contact (grounding) caused variable amounts of basal traction, which was parameterized by a Weertman sliding law, providing a commonly adopted relation between the basal sliding velocity v_b and basal shear stress τ_b in grounded areas, $\boldsymbol{\tau_b = C^{-1/m}\|v_b\|^{\frac{1}{m}-1}v_b}$, with m and C model parameters. A common value for the sliding exponent $m = 3$ was chosen, and the slipperiness coefficient was tuned to $C = 10^{-3}$ in order to produce the best fit between the amplitudes of observed and modelled changes in surface speed after 10 years (Figure 4b).

The striking similarities between the observed and modelled patterns of change in Figure 4b provides a powerful validation for the predictive skill of Úa and, consequently, for models with a comparative representation of ice dynamics. To our knowledge, this is the first successful back-testing of a numerical ice-flow model against observed transient changes in ice-flow velocities of an Antarctic ice shelf.

At present, however, ice-flow models do not generally incorporate a physical mechanism for fracture initiation and propagation, and changes during the stress-release (or calving) phase of ice-shelf evolution cannot be simulated. In contemporary model studies, the ice front is often fixed to its present-day configuration, and the natural cycle of ice-shelf

growth followed by singular calving events is assumed unimportant at decadal to centennial time scales. Our observations and the above model results show that this can be a very poor assumption.

In order to quantitatively assess the impact of these model shortcomings, we continued transient simulation of the BIS for 8 more years (2011 to 2018), and compared model results in the absence of rifting to velocity observations from October 2018. During this time period, Chasm 1 and the Halloween Crack propagated as shown in Figure 4c, and caused a loss of buttressing and widespread speed-up of the ice shelf. However, modeled surface speeds in the absence of rifting remained largely constant or slightly decreased between 2011 and 2018 (Figure 4c). As a consequence, model simulations underestimate the flow speed upstream of Chasm 1 by up to 25%, and by 100% on sections that became partly disconnected from the main ice shelf.

7 Concluding remarks

Our results, based on observations and numerical modelling, unequivocally demonstrate the need for a calving law that links large-scale changes in ice shelf configuration to fracture mechanics. Such developments are currently underway, e.g. (Lipovsky, 2018b), but have not been implemented into flow models. Existing calving criteria based on a minimum ice thickness, such as the ice-cliff instability mechanism (De Conto and Pollard, 2016), have yet to be validated against direct observations, and these discard variations in mechanical properties of the ice. Other calving laws are formulated as a criterion for the vertical propagation of surface and basal crevasses (Hughes, 1983, van der Veen, 1998a, 1998b), often linked to surface hydrology (Scambos et al, 2000, Scambos et al., 2009, Nick et al., 2013), but do not generally include criteria for the initiation and horizontal propagation of full-depth rifts. As a result, model simulations do not generally capture rapid and large-scale changes in ice shelf geometry, and thereby underestimate the critical role of ice shelves as a buffer against further mass loss from the Antarctic Ice Sheet.

Code and data availability

All satellite data is available through the ENVEO Cryoportal (cryoportal.enveo.at), GPS data will be made available through the UK Polar Data Centre (DOI tbc), the source code of the ice flow model Úa is available from https://github.com/ghilmarg; results from the model inversions will be made available through the UK Polar Data Centre (DOI tbc). All requests for data and model outputs should be addressed to J.D.R. (jan.rydt@northumbria.ac.uk).

Author contributions

J.D.R. and G.H.G. designed and initiated the project; T.N. and J.W. processed the satellite data; G.H.G. and J.D.R. were responsible for in-situ data collection, processing and quality control; J.D.R. performed the model simulations, carried out the data analysis and prepared the figures and manuscript; G.H.G., T.N. and J.W. reviewed and edited the manuscript.

Competing interests

The authors declare no competing interests.

Acknowledgements

We acknowledge the UK's Natural Environmental Research Council for providing us with the in-situ GPS data. T.N. and J.W. acknowledge support from the European Space Agency (ESA) through the ESA Antarctic Ice Sheet CCI program and from ASAP (Austrian Space Application Programme).

References

Anderson, R., Jones, D. H. and Gudmundsson, G. H.: Halley Research Station, Antarctica: calving risks and monitoring strategies, Natural Hazards and Earth System Sciences, 14, 917–927, 2014.

Bassis, J. N., Coleman, R., Fricker, H. A. and Minster, J. B.: Episodic propagation of a rift on the Amery Ice Shelf, East Antarctica, Geophysical Research Letters, 32, 2005.

Bassis, J. N., Fricker, H. A., Coleman, R. and Minster, J.-B.: An investigation into the forces that drive ice-shelf rift propagation on the Amery Ice Shelf, East Antarctica, Journal of Glaciology, 54, 17–27, 2008.

Bindschadler, R.et al.: Getting around Antarctica: new high-resolution mappings of the grounded and freely-floating boundaries of the Antarctic ice sheet created for the International Polar Year, The Cryosphere 5, 569–588, 2011.

Borstad, C., McGrath, D. and Pope, A.: Fracture propagation and stability of ice shelves governed by ice shelf heterogeneity, Geophysical Research Letters, 44, 4186–4194, 2017.

Cuffey, K. and Paterson, W.: The physics of glaciers (Academic Press, 2010), fourth edn.

De Conto, R. M. and Pollard, D.: Contribution of Antarctica to past and future sea-level rise, Nature, 531, 591–597, 2016.

De Rydt, J., Gudmundsson, G. H., Nagler, T., Wuite, J. and King, E. C.: Recent rift formation and impact on the structural integrity of the Brunt Ice Shelf, East Antarctica, The Cryosphere, 12, 505–520, 2018.

Depoorter, M. A. et al.: Calving fluxes and basal melt rates of Antarctic ice shelves, Nature, 502, 89–92, 2013.

Doake, C. S. M., Corr, H. F. J., Rott, H., Skvarca, P. and Young, N. W.: Breakup and conditions for stability of the northern Larsen Ice Shelf, Antarctica, Nature, 391, 778–780, 1998.

Dupont, T. K. and Alley, R. B.: Assessment of the importance of ice-shelf buttressing to ice-sheet flow, Geophysical Research Letters, 32, 2005.

Engwirda, D.: Locally-optimal Delaunay-refinement and optimisation-based mesh generation. Ph.D. thesis, School of Mathematics and Statistics, The University of Sydney, 2014.

Flament, T. and Rémy, F.: Dynamic thinning of Antarctic glaciers from along-track repeat radar altimetry, Journal of Glaciology, 58, 830–840, 2012.

Fretwell, P. et al.: Bedmap2: improved ice bed, surface and thickness datasets for Antarctica, The Cryosphere 7, 375–393, 2013.

Fürst, J. J.et al.: The safety band of Antarctic ice shelves. Nature Climate Change 6, 479–782, 2016.

Gudmundsson, G. H., De Rydt, J. and Nagler, T.: Five decades of strong temporal variability in the flow of Brunt Ice Shelf, Antarctica, Journal of Glaciology, 63, 164–175, 2017.

Gudmundsson, G. H., Krug, J., Durand, G., Favier, L. and Gagliardini, O.: The stability of grounding lines on retrograde slopes, The Cryosphere, 6, 1497–1505, 2012.

Hodgson, D. A.et al.: Past and future dynamics of the Brunt Ice Shelf from seabed bathymetry and ice shelf geometry, The Cryosphere, 13, 545-556, 2019.

Hogg, A. E. and Gudmundsson, G. H.: Impacts of the Larsen-C ice shelf calving event, Nature Climate Change, 7, 540, 2017.

Howat, I. M., Porter, C., Smith, B. E., Noh, M.-J. and Morin, P.: The reference elevation model of Antarctica. The Cryosphere, 13, 665-674, 2019.

Hughes, T.: On the Disintegration of Ice Shelves: The Role of Fracture, Journal of Glaciology, 29, 98–117, 1983.

Khazendar, A., Rignot, E. and Larour, E.: Roles of marine ice, rheology, and fracture in the flow and stability of the Brunt/Stancomb-Wills Ice Shelf, Journal of Geophysical Research: Earth Surface, 114, 2009.

King, E. C., De Rydt, J. and Gudmundsson, G. H.: The internal structure of the Brunt Ice Shelf from ice-penetrating radar analysis and implications for ice shelf fracture, The Cryosphere, 12, 3361–3372, 2018.

Konrad, H. et al.: Uneven onset and pace of ice-dynamical imbalance in the Amundsen Sea Embayment, West Antarctica, Geophysical Research Letters, 44, 910–918, 2016.

Lipovsky, B. P.: Ice Shelf Rift Propagation and the Mechanics of Wave-Induced Fracture, Journal of Geophysical Research: Oceans, 123, 4014–4033, 2018a.

Lipovsky, B. P.: Ice shelf stability and the brittle–ductile transition, 2018b. URL: eartharxiv.org/5b9y4.

Mouginot, J., Rignot, E., Scheuchl, B. and Millan, R.: Comprehensive annual ice sheet velocity mapping using Landsat-8, Sentinel-1, and RADARSAT-2 data, Remote Sensing, 9, 2017.

Nagler, T., Rott, H., Hetzenecker, M., Wuite, J. and Potin, P.: The sentinel-1 mission: New opportunities for ice sheet observations, Remote Sensing 7, 9371–9389, 2015.

Nicholls, K. W., Østerhus, S., Makinson, K., Gammelsrød, T. and Fahrbach, E.: Ice-ocean processes over the continental shelf of the southern Weddell Sea, Antarctica: A review, Reviews of Geophysics, 47, 2009.

Nick F. M. et al.: Future sea-level rise from Greenland's main outlet glaciers in a warming climate, Nature, 497, 235–238, 2013.

Paolo, F. S., Fricker, H. A. and Padman, L.: Volume loss from Antarctic ice shelves is accelerating, Science, 348, 327–331, 2015.

Pritchard, H. D., Arthern, R. J., Vaughan, D. G. and Edwards, L. A.: Extensive dynamic thinning on the margins of the Greenland and Antarctic ice sheets, Nature, 461, 971–975, 2009.

Pritchard, H. D., Ligtenberg S. R. M., Fricker H. A., Vaughan D. G., van den Broeke, M. R. And Padman L.: Antarctic ice-sheet loss driven by basal melting of ice shelves, Nature, 484, 502-505, 2012.

Reeh, N.: On the calving of ice from floating glaciers and ice shelves, Journal of Glaciology, 7, 215–232, 1968.

Reese, R., Winkelmann, R. and Gudmundsson, G. H.: Grounding-line flux formula applied as a flux condition in numerical simulations fails for buttressed Antarctic ice streams, The Cryosphere 12, 3229–3242, 2018.

Rignot, E. et al.: Accelerated ice discharge from the Antarctic Peninsula following the collapse of Larsen B ice shelf, Geophys. Res. Lett., 31, L18401, 2004.

Rist, M. A., Sammonds, P. R., Oerter, H. and Doake, C. S. M.: Fracture of Antarctic shelfice, Journal of Geophysical Research: Solid Earth, 107, 2002.

Rott, H., Müller, F., Nagler, T. and Floricioiu, D.: The imbalance of glaciers after disintegration of Larsen-B ice shelf, Antarctic Peninsula, The Cryosphere, 5, 125–134, 2011.

Scambos, T. A., Bohlander, J. A., Shuman, C. A. and Skvarca, P.: Glacier acceleration and thinning after ice shelf collapse in the Larsen B embayment, Antarctica, Geophysical Research Letters, 31, 2004.

Scambos, T. A., Hulbe, C., Fahnestock, M. and Bohlander, J.: The link between climate warming and break-up of ice shelves in the Antarctic Peninsula, Journal of Glaciology, 46, 516–530, 2000.

Scambos, T.et al.: Ice shelf disintegration by plate bending and hydro-fracture: Satellite observations and model results of the 2008 Wilkins ice shelf break-ups, Earth and Planetary Science Letters, 280, 51 – 60, 2009.

Simmons, D. and Rouse, J.: Accelerating flow of the Brunt Ice Shelf, Antarctica, Journal of Glaciology, 30, 377–380, 1984.

Simmons, D.: Flow of the Brunt Ice Shelf, Antarctica, Derived from Landsat Images, 1974–85, Journal of Glaciology, 32, 252–254, 1986.

Slater, T. et al.: A new digital elevation model of Antarctica derived from CryoSat-2 altimetry, The Cryosphere, 12, 1551–1562, 2018.

Thomas, R. H.: The creep of ice shelves: Interpretation of observed behaviour, Journal of Glaciology, 12, 55–70, 1973.

van der Veen, C.: Fracture mechanics approach to penetration of surface crevasses on glaciers, Cold Regions Science and Technology, 27, 31 – 47, 1998a.

van der Veen, C.: Fracture mechanics approach to penetration of bottom crevasses on glaciers, Cold Regions Science and Technology, 27, 213 – 223, 1998b.

Wouters, B. et al.: Dynamic thinning of glaciers on the Southern Antarctic Peninsula, Science, 348, 899–903, 2015.

The Cryosphere Discuss., https://doi.org/10.5194/tc-2019-46
Manuscript under review for journal The Cryosphere
Discussion started: 3 April 2019

The Cryosphere Discussions
Open Access
EGU

Figure 1: Map of the Brunt Ice Shelf with inset showing its location in relation to the Antarctic continent (Howat et al., 2019). Panel a shows the ice shelf in 2010, prior to rifting. The grounding lines (solid black lines, (Bindschadler et al., 2011)), open ocean shaded in blue, and surface velocities from the MEaSUREes 2010-2011 annual Antarctic velocity map (white arrows, (Mouginot et al., 2017)), are overlain on a Landsat-7 panchromatic image collected on 4 January 2010. All velocity maps in this study have been cross-calibrated to data from a network of up to 15 in situ GPS stations. The configuration of the network in 2010 is shown by the yellow dots, with corresponding velocity arrows in black. Panel b shows the extent of two active rifts – 'Chasm 1' and the 'Halloween Crack' – in October 2018, with cyan arrows indicating their direction of propagation. Black arrows represent velocity anomalies between 2010, prior to rift initiation, and February 2018 (Sentinel-1 data), showing a dramatic increase in flow as a result of ice-shelf rifting. Blue-to-red colors illustrate the corresponding change in surface speed. Ice front locations in 1978, 2010 and 2018 are shown for reference.

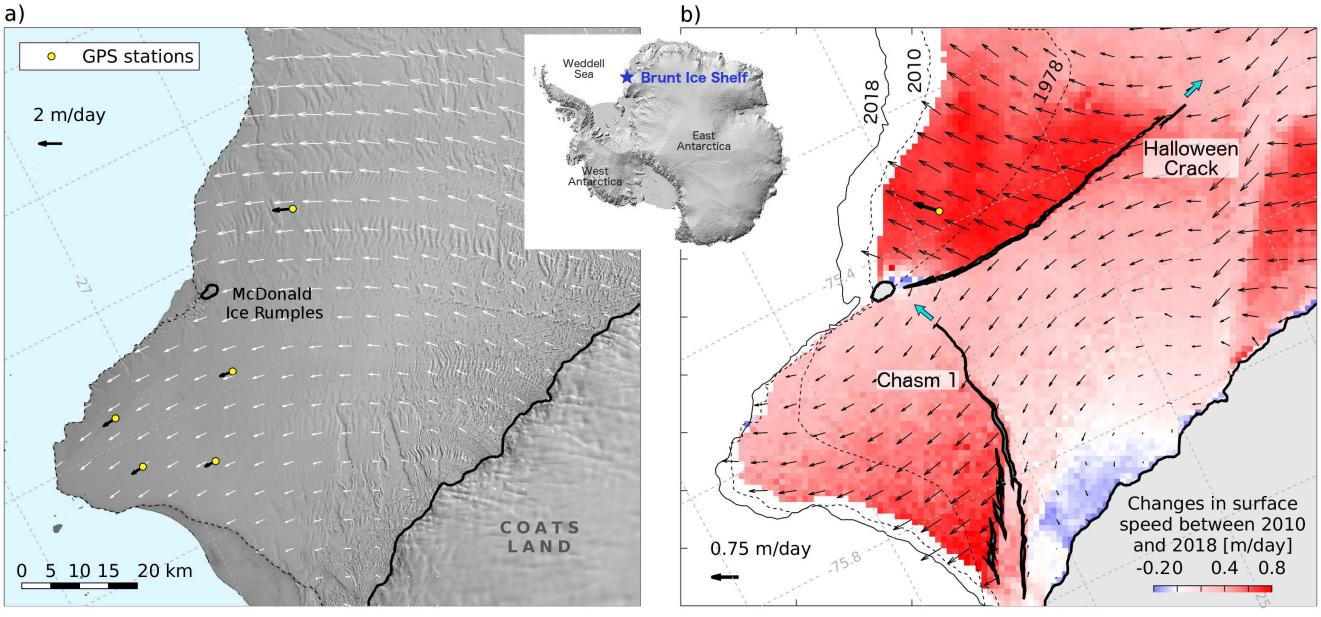

The Cryosphere Discuss., https://doi.org/10.5194/tc-2019-46
Manuscript under review for journal The Cryosphere
Discussion started: 3 April 2019

Figure 2: Temporal evolution of principal deviatoric stress components (black arrows for extension, red arrows for compression) and maximum deviatoric stress amplitude (colours) as the Brunt Ice Shelf re-grounds at the McDonald Ice Rumples. The blue marker in panel c indicates the historical tip of Chasm 1, which corresponds to the onset location of rift propagation in December 2012. The blue marker in the panel d shows the onset location of the Halloween Crack on 4 October 2016. Panels are dated with the time stamp of the corresponding surface velocity used in the diagnostic calculation of the stress field (Table 1). Black boxes in panel d indicate the geographical extent of panels in Figure 3.

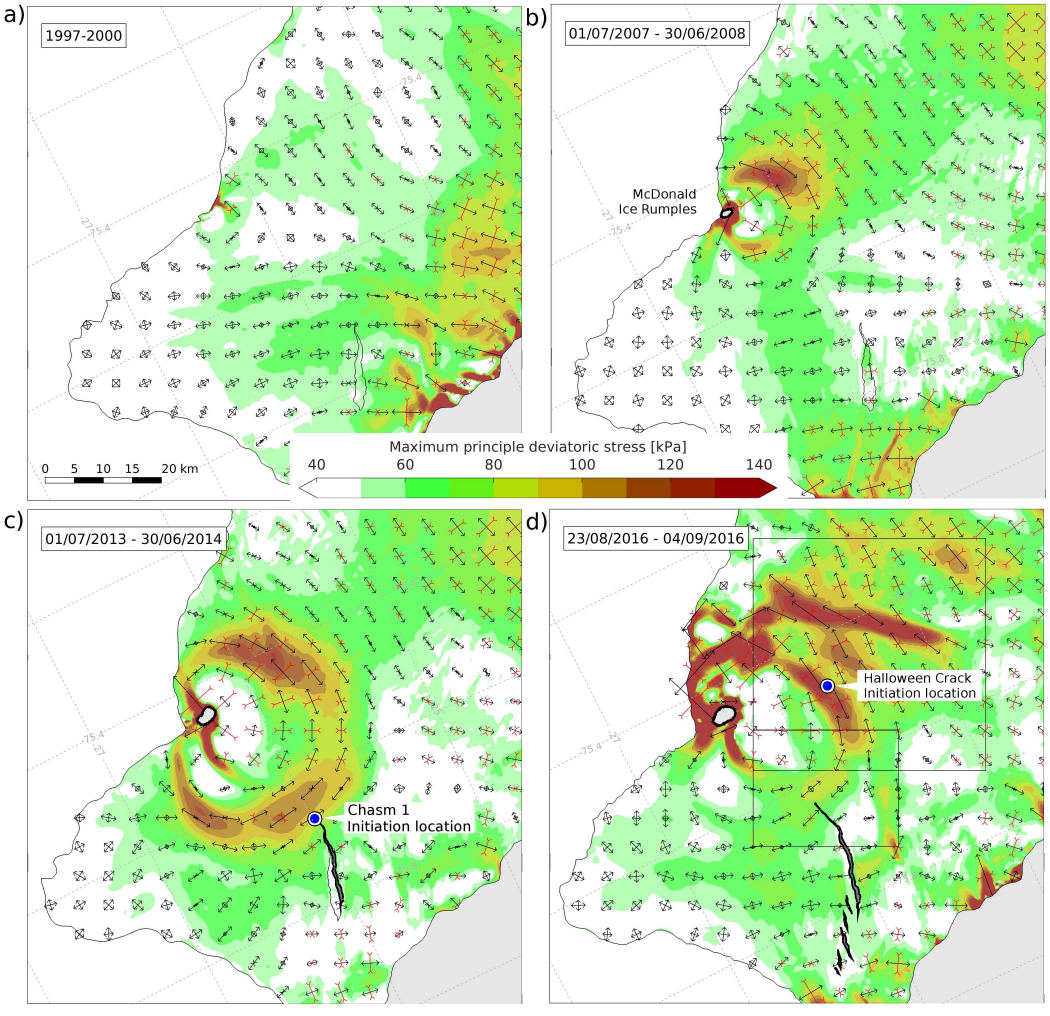

The Cryosphere Discuss., https://doi.org/10.5194/tc-2019-46
Manuscript under review for journal The Cryosphere
Discussion started: 3 April 2019

Figure 3: An effective demonstration of the reduction in tensile stress following rift propagation. Top row: the Halloween Crack remained stagnant for most of November 2016 resulting in the localized accumulation of stress, before propagating 11 km in December 2016 and causing a significant release of stress. Bottom row: Chasm 1 lengthened by only 500 m in 2016 compared to 1.5 km/yr in preceding years, and by January 2017, a zone of high tensile stress developed ahead of the rift tip (panel c). This zone intensified by May 2017 (panel d) and tension dissipated by October 2017 (panel e), following a rapid progression by 4.5 km. For reference, the blue markers indicate the location of rift initiation as in Figure 2, and the dashed contours panels b and e correspond to the stresses before propagation.

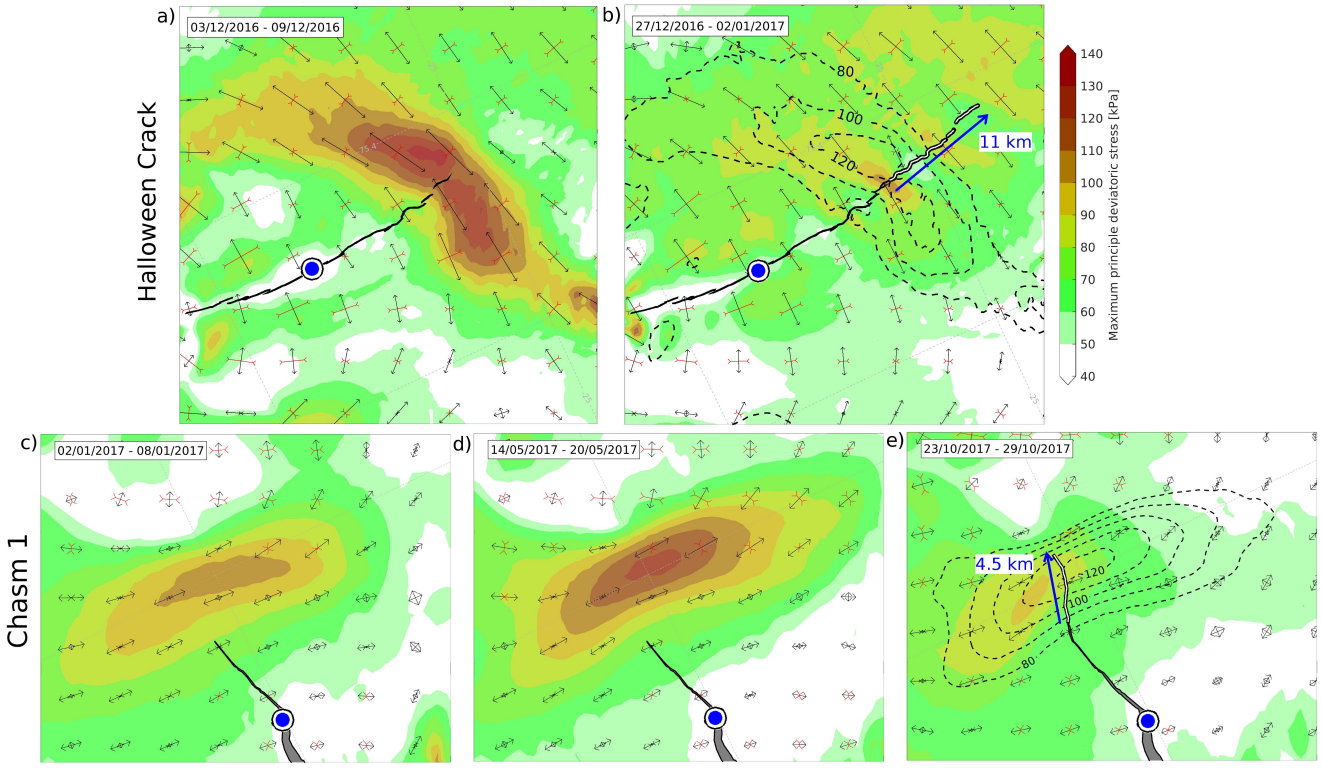

The Cryosphere Discuss., https://doi.org/10.5194/tc-2019-46
Manuscript under review for journal The Cryosphere
Discussion started: 3 April 2019

Figure 4: Comparison between observed (left column) and modelled (right column) surface speed of the Brunt Ice Shelf between 2000 and 2018. The 2000 ice front location is shown by the dashed lines and the extent of the McDonald Ice Rumples is shaded in grey. Observations and model simulations broadly agree in 2000, and both show a significant slow-down between 2000 and 2011due to increasing contact between the ice-shelf draft and a seabed shoal at the McDonald Ice Rumples. However, observations and model simulations strongly diverge after the formation and propagation of Chasm 1 (2012) and the Halloween Crack (2016). This difference is because Chasm1 is not generated within the numerical model due to the model's lack of a fracture mechanical component. This situation is typical for current generation of large-scale ice shelf models. Here, these differences lead to ice flow speed being underestimated by more than 1 m/day (or up to 100%) at the end of a transient run over less than a decade.

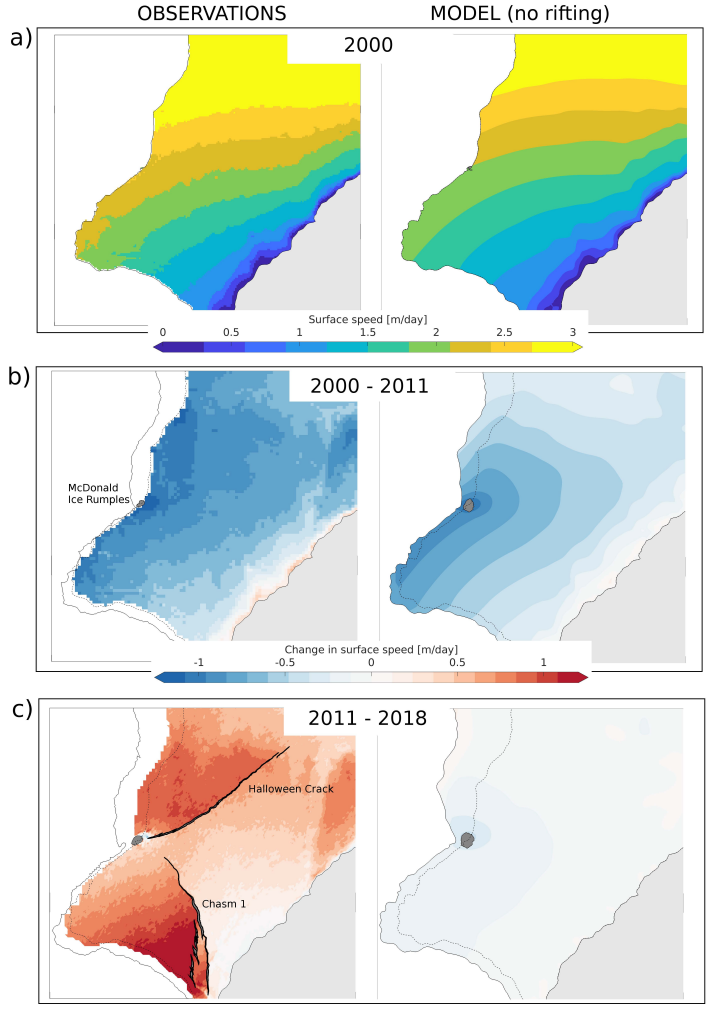

The Cryosphere Discuss., https://doi.org/10.5194/tc-2019-46
Manuscript under review for journal The Cryosphere
Discussion started: 3 April 2019

Table 1. Data sources and corresponding timestamps used for the stress calculations. The effective timestamp in the first column corresponds to the middle of the velocity feature tracking window, and WorldView-2 surface elevations were shifted to the corresponding effective time stamp.

Effective time stamp	Surface DEM	Surface velocity	Ice front location
01/01/1999	Bedmap 2 *(Fretwell et al., 2013)*	RADARSAT1 *(Khazendar et al., 2009)* 1997-2001	Landsat 7 14/02/2001
01/01/2008	WorldView-2	MEaSUREs *(Mouginot et al., 2017)* 01/07/2007 – 30/06/2008	Landsat 7 18/12/2007
01/01/2014	WorldView-2	MEaSUREs 01/07/2013 – 30/06/2014	Landsat 7 04/01/2014
29/08/2016	WorldView-2	Sentinel-1A/B 23/08/2016 – 04/09/2016	Landsat 8 29/09/2016
06/12/2016	WorldView-2	Sentinel-1A/B 03/12/2016 – 09/12/2016	Landsat 8 09/12/2016
30/12/2016	WorldView-2	Sentinel-1A/B 27/12/2016 – 02/01/2017	Landsat 8 01/01/2017
06/01/2017	WorldView-2	Sentinel-1A/B 02/01/2017 – 08/01/2017	Landsat 8 01/01/2017
17/05/2017	WorldView-2	Sentinel-1A/B 14/05/2017 – 20/05/2017	Landsat 8 15/03/2017
27/10/2017	WorldView-2	Sentinel-1A/B 27/10/2017 – 29/10/2017	Landsat 8 25/10/2017